

## Supporting information

### Charge transport enhancement in supramolecular oligothiophene assemblies using Pt(II) centers as a guide

Amparo Ruiz-Carretero,<sup>\*[a,e]</sup> Youssef Atoini,<sup>[a]</sup> Tianyan Han,<sup>[b]</sup> Alessandra Operamolla,<sup>[c]</sup> Stefano Ippolito,<sup>[d]</sup> Cataldo Valentini,<sup>[c, f]</sup> Serena Carrara,<sup>[a, g]</sup> Stephan Sinn,<sup>[a, h]</sup> Eko Adi Prasetyanto,<sup>[a, i]</sup> Thomas Heiser,<sup>[b]</sup> Paolo Samorì,<sup>[d]</sup> Gianluca Farinola,<sup>[c]</sup> Luisa De Cola<sup>\* [a, h]</sup>

---

[a] Dr. A. Ruiz-Carretero, Dr. Y. Atoini, Dr. S. Sinn Dr. E. A. Prasetyanto, Dr. S. Carrara, Prof. L. De Cola. University of Strasbourg, CNRS, ISIS, Laboratory of Supramolecular Biomaterials and Chemistry, 8 allée Gaspard Monge, 67000 Strasbourg, France.

[b] Dr. Tianyan Han, Prof. Thomas Heiser. ICube, Equipe MaCEPV. 23 rue du Loess, 67037, Strasbourg Cedex 02, France.

[c] Dr. A. Operamolla, Dr. C. Valentini, Prof. G. Farinola. Dipartimento di Chimica. Università degli Studi di Bari Aldo Moro. Via Orabona 4. I-70126 Bari, Italy.

[d] Stefano Ippolito, Prof. Paolo Samorì. University of Strasbourg, CNRS, ISIS, Nanochemistry Laboratory, 8 allée Gaspard Monge, 67000 Strasbourg, France.

[e] Current affiliation: University of Strasbourg, CNRS, Institut Charles Sadron. 23 Rue de Loess, BP 84047, 67034 Strasbourg, Cedex 2. France.

[f] Current affiliation: Cardiff University Main Building, Park Pl, CF10 3AT, Cardiff (UK)

[g] Current affiliation: Aix Marseille Université, CNRS, CINAM, 163 Avenue de Luminy, case 913, 13009 Marseille, France.

[h] Karlsruhe Institute of Technology (KIT), Institute of Nanotechnology, Hermann-von-Helmholtz-Platz. 76344 Eggenstein-Leopoldshafen, Germany.

[i] Current affiliation: Atma Jaya Catholic University of Indonesia. Jakarta, Indonesia

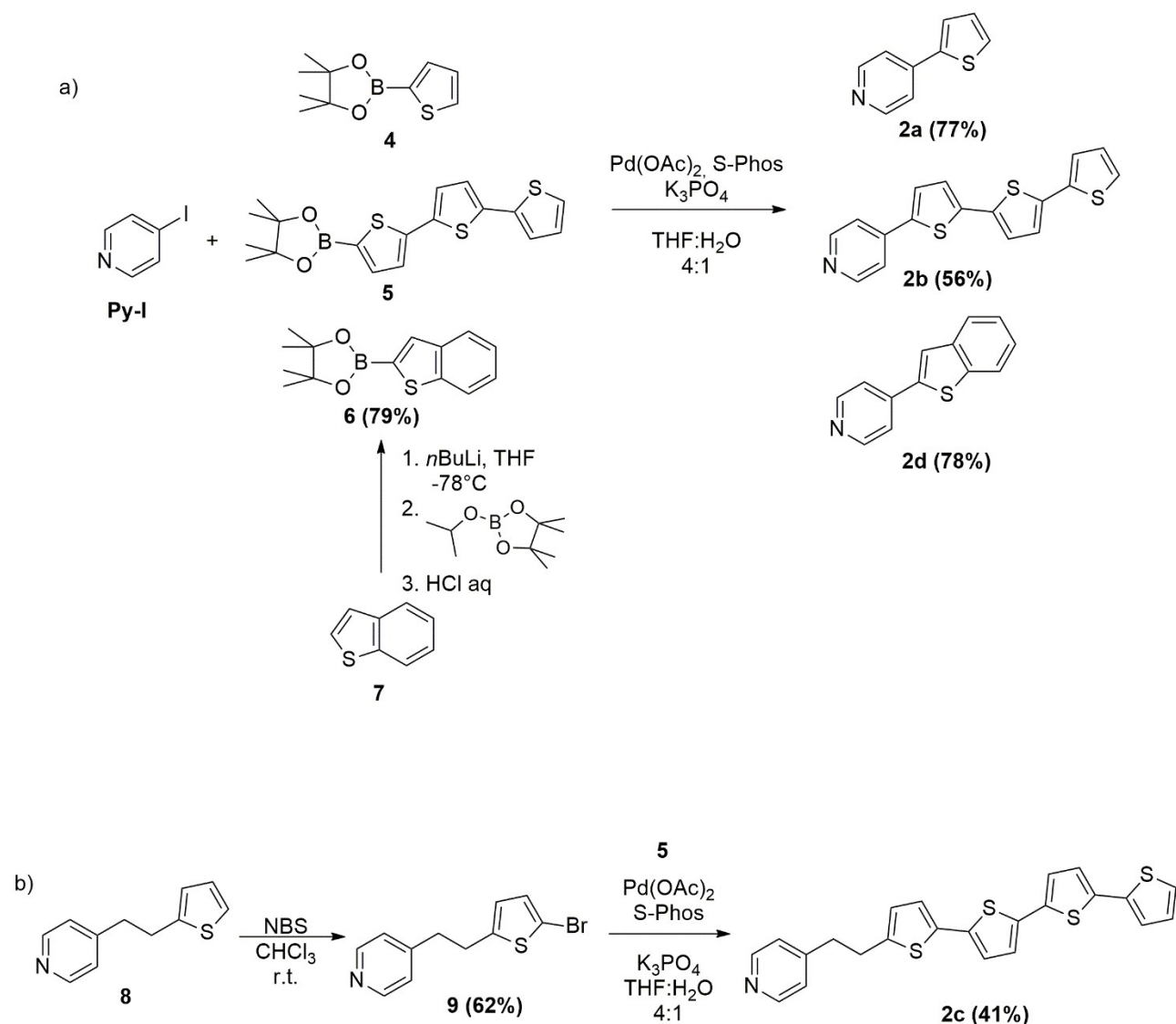
\*Corresponding authors. E-mail: ruizcarretero@unistra.fr, [decola@unistra.fr](mailto:decola@unistra.fr).

## Synthesis of 2a-d ligands

**General:** All reactions were carried out under a nitrogen atmosphere in oven-dried glassware, with dry solvents, unless otherwise stated. THF and toluene were distilled immediately prior to use from sodium/benzophenone. Reagents were purchased at the highest commercial quality and used without further purification. Anhydrous tribasic potassium phosphate was finely ground prior to use. Compounds 4-7 were commercial products. 4-(2-(thiophen-2-yl)ethyl)pyridine **8** was synthesized according to reference 1. Microwave assisted reactions were carried out in a sealed teflon tube on a Milestone MicroSynth microwave oven equipped with a temperature probe. Preparative column chromatography was carried out using Macherey-Nagel silica gel (60, particle size 0.063-0.2 mm). Macherey-Nagel aluminum sheets with silica gel 60 F254 were used for TLC analyses. All new compounds were characterized by <sup>1</sup>H-NMR, <sup>13</sup>C-NMR spectroscopies and HMRS spectrometry. <sup>1</sup>H and <sup>13</sup>C NMR spectra were recorded on a Varian Inova at 400 and at 100.6 MHz, respectively, by using the residual proton peak of CDCl<sub>3</sub> at  $\delta$  = 7.26 ppm as internal standard for <sup>1</sup>H spectra and the signals of CDCl<sub>3</sub> at  $\delta$  = 77 ppm as internal standard for <sup>13</sup>C spectra. Coupling constants values J are given in Hz. High-resolution mass spectra were acquired on a Shimadzu high performance liquid chromatography-ion trap-time of flight mass spectrometer (LCMS-IT-TOF) via direct infusion of the samples using acetonitrile as the elution solvent. Melting points (uncorrected) were determined on a Reichert Microscope.

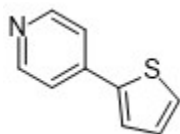
### Synthetic methods for ligands 2a-d

The ancillary ligands **2a-d** were synthesized according to the following Scheme S1. Synthetic details and characterization are reported below.



**Scheme 1.** Synthesis of compounds **2a-d**

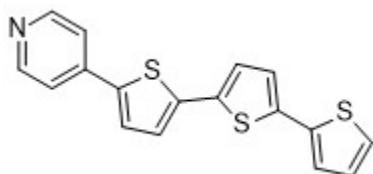
#### 4-(thiophen-2-yl)pyridine **2a**



A 50 mL three necked round bottom flask was conditioned with nitrogen and charged with thiophen-2-ylboronic acid (1.620 g, 7.3 mmol), 4-iodopyridine (1.000 g, 4.9 mmol), THF (30 mL) and distilled water (7.5 mL). The resulting mixture was degassed by bubbling nitrogen for 15 minutes. Then the catalysts  $\text{Pd(OAc)}_2$  (10 mg, 0.04 mmol), S-Phos (36 mg, 0.09 mmol), the base  $\text{K}_3\text{PO}_4$  (1.000 g, 4.5 mmol) and Aliquat 3,3,6 (5 drops) were added and the resulting dark

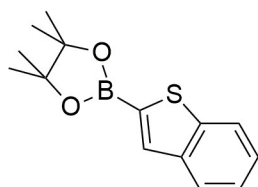
solution was transferred, using a syringe and a needle, to a microwave teflon reaction tube. The tube was sealed and put into a microwave oven. The mixture was irradiated with a power of 200W until the temperature of 160°C was reached and maintained for 15 minutes, then it was allowed to reach room temperature. The solvent was evaporated under reduced pressure. The residue was diluted with NaHCO<sub>3</sub>aq 10% (30 mL) and extracted with dichlorometane (3 x 40 mL). The organic extracts were collected, dried over anhydrous Na<sub>2</sub>SO<sub>4</sub> and filtered off. The solvent was removed under reduced pressure and the crude material was purified by column chromatography on silica gel, eluting with a solvent mixture of AcOEt:Et<sub>3</sub>N in volumetric ratio 99:1. A white solid (605 mg) was isolated with a yield of 77%. Mp (Lit.<sup>2</sup> 93-94°C): 92.7-93.9°C. <sup>1</sup>H NMR (400 MHz, CDCl<sub>3</sub>) δ= 8.59 (dd, J = 4.6, 1.7 Hz, 2H), 7.51 (dd, J = 3.7, 1.1 Hz, 1H), 7.48 (dd, J = 4.6, 1.7 Hz, 2H), 7.41 (dd, J = 5.1, 1.0 Hz, 1H), 7.14 (dd, J = 5.1, 3.7 Hz, 1H).

#### 4-([2,2':5',2''-terthiophen]-5-yl)pyridine 2b



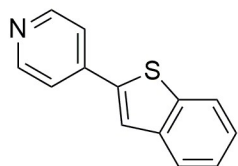
A 50 mL three necked round bottom flask was conditioned with nitrogen and charged with 2-([2,2':5',2''-terthiophen]-5-yl)-4,4,5,5-tetramethyl-1,3,2-dioxaborolane (657 mg, 1.8 mmol), 4-iodopyridine (300 mg, 1.5 mmol), THF (20 mL) and distilled water (4 mL). The resulting mixture was degassed by bubbling nitrogen for 15 minutes. Then the catalysts Pd(OAc)<sub>2</sub> (16 mg, 0.08 mmol), S-Phos (60 mg, 0.15mmol) and the base K<sub>3</sub>PO<sub>4</sub> (1.300 g, 5.8 mmol) were added and the resulting dark solution was transferred, using a syringe and a needle, to a microwave teflon reaction tube. The tube was sealed and put into a microwave oven. The mixture was irradiated with a power of 200W until the temperature of 160°C was reached and maintained for 20 minutes, then it was allowed to reach room temperature. The solvent was evaporated under reduced pressure. The residue was diluted with NaHCO<sub>3</sub>aq 10% (15 mL) and extracted with dichlorometane (3 x 20 mL). The organic extracts were collected, dried over anhydrous Na<sub>2</sub>SO<sub>4</sub> and filtered off. The solvent was removed under reduced pressure and the crude material was purified by column chromatography on silica gel, eluting with a solvent mixture of CH<sub>2</sub>Cl<sub>2</sub>:MeOH:Et<sub>3</sub>N in volumetric ratio 94:5:1. A white solid (265 mg) was isolated with a yield of 56%. Mp (Lit.<sup>3</sup> 239°C): 237.3-238.5°C. <sup>1</sup>H NMR (400 MHz, CDCl<sub>3</sub>) δ = 8.60 (dd, J = 4.5, 1.6 Hz, 2H), 7.46 (dd, J = 4.5, 1.6 Hz, 2H), 7.43 (d, J = 3.9 Hz, 1H), 7.25 (dd, J = 1.1 Hz, J = 1H), 7.20 (dd, J = 3.6, 1.1 Hz, 1H), 7.19 (d, J = 3.9 Hz, 1H), 7.16 (d, J = 3.8 Hz, 1H), 7.11 (d, J = 3.8 Hz, 1H), 7.04 (dd, J = 5.1, 3.6 Hz, 1H).

#### 2-(benzo[b]thiophen-2-yl)-4,4,5,5-tetramethyl-1,3,2-dioxaborolane 7



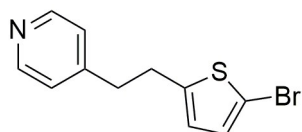
A 100 mL three necked round bottom flask was charged with benzo[b]thiophene (1.0 g, 7.5 mmol) and conditioned with nitrogen. THF (25 mL) was added and the resulting solution was cooled to  $-78^{\circ}\text{C}$ . 3.28 mL of *n*BuLi (2.5 M solution in hexane) were added dropwise to the mixture and the system was kept at  $-78^{\circ}\text{C}$  for further 30'. After that, 3.1 mL (15 mmol) of 2-isopropoxy-4,4,5,5-tetramethyl-1,3,2-dioxaborolane were added dropwise and the system was slowly allowed to reach room temperature. After 16h total reaction time, the mixture was quenched by addition of 10 mL of a saturated  $\text{NH}_4\text{Cl}$  solution and the solvent was distilled under reduced pressure. The residue was diluted with water (50 mL) and extracted with hexane (3 x 70 mL). The organic extracts were collected, washed with brine (2 x 30 mL), dried over anhydrous  $\text{Na}_2\text{SO}_4$  and filtered off. The solvent was removed under reduced pressure and the crude material was purified by crystallization from methanol and water (two times). A white solid (1.527 g) was isolated (79% yield). Mp (Lit.<sup>4</sup> colorless oil):  $178\text{-}180^{\circ}\text{C}$ .  $^1\text{H}$  NMR (400 MHz,  $\text{CDCl}_3$ )  $\delta$  = 7.87-7.63 (m, 3H), 7.34-7.23 (m, 2H), 1.26 (s, 12H).

#### 4-(benzo[b]thiophen-2-yl)pyridine 2d



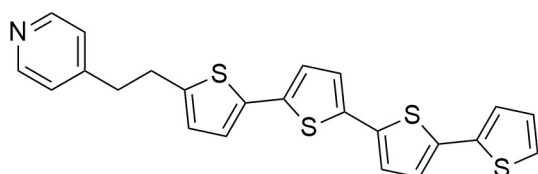
A 25 mL three necked round bottom flask was conditioned with nitrogen and charged with 2-(benzo[b]thiophen-2-yl)-4,4,5,5-tetramethyl-1,3,2-dioxaborolane (330 mg, 1.3 mmol), 4-iodopyridine (200 mg, 1.0 mmol), toluene (10 mL) and distilled water (3 mL). The resulting mixture was degassed by bubbling nitrogen for 15 minutes. Then the catalysts  $\text{Pd}(\text{OAc})_2$  (11 mg, 0.05 mmol), S-Phos (40 mg, 0.10 mmol), the base  $\text{K}_3\text{PO}_4$  (870 mg, 3.9 mmol) and Aliquat 3,3,6 (4 drops) were added and the resulting dark solution was transferred, using a syringe and a needle, to a microwave teflon reaction tube. The tube was sealed and put into a microwave oven. The mixture was irradiated with a power of 200W until the temperature of  $150^{\circ}\text{C}$  was reached and maintained for 10 minutes, then it was allowed to reach room temperature. The solvent was evaporated under reduced pressure. The residue was diluted with  $\text{NaHCO}_3$  aq 10% (15 mL) and extracted with dichloromethane (3 x 30 mL). The organic extracts were collected, dried over anhydrous  $\text{Na}_2\text{SO}_4$  and filtered off. The solvent was removed under reduced pressure and the crude material was purified by column chromatography on silica gel, eluting with a solvent mixture of hexane:AcOEt:Et<sub>3</sub>N in volumetric ratio 49:50:1. A white solid (161 mg) was isolated with a yield of 78%. Mp (Lit.<sup>5</sup>  $171^{\circ}\text{C}$ ):  $171^{\circ}\text{C}$  (phase transition);  $191.9\text{-}194.0^{\circ}\text{C}$  (melting process).  $^1\text{H}$  NMR (400 MHz,  $\text{CDCl}_3$ )  $\delta$  8.65 (dd,  $J$  = 4.6, 1.6 Hz, 2H), 7.90 – 7.79 (m, 2H), 7.75 (s, 1H), 7.63 – 7.54 (m, 2H), 7.43 – 7.34 (m, 2H).

#### 4-(2-(5-bromothiophen-2-yl)ethyl)pyridine 9



A 50 mL round bottom flask was charged with 4-(2-(thiophen-2-yl)ethyl)pyridine (388 mg), N-bromosuccinimide (245 mg) and chloroform (10 mL). The resulting mixture was stirred in the dark at room temperature until the disappearance of the starting product was observed by TLC. The solvent was distilled under reduced pressure, and the residue was purified by washing with hot hexane (three times). A brown solid (339 mg) was isolated with a yield of 73%. Mp: the product starts decomposing at 41°C. <sup>1</sup>H NMR (400 MHz, CDCl<sub>3</sub>) δ 8.56 – 8.47 (m, 2H), 7.09 (d, J = 5.9 Hz, 2H), 6.83 (d, J = 3.6 Hz, 1H), 6.49 (d, J = 3.7 Hz, 1H), 3.08 (t, J = 7.6 Hz, 2H), 2.93 (t, J = 7.6 Hz, 2H). <sup>13</sup>C NMR (95 MHz, CDCl<sub>3</sub>) δ 149.1, 142.6, 137.0, 135.3, 127.9, 125.8, 124.17, 123.4, 37.0, 30.7. [M+H]<sup>+</sup> Calc for C<sub>11</sub>H<sub>10</sub>BrNS 267.9790, Found 267.9783, 269.9764 [M+2+H]<sup>+</sup>.

#### 4-(2-([2,2':5',2'':5'',2'''-quaterthiophen]-5-yl)ethyl)pyridine 2c



A 25 mL three necked round bottom flask was conditioned with nitrogen and charged with 2-([2,2':5',2'':5'',2'''-terthiophen]-5-yl)-4,4,5,5-tetramethyl-1,3,2-dioxaborolane (337 mg, 0.9 mmol), 4-(2-(5-bromothiophen-2-yl)ethyl)pyridine (200 mg, 0.75 mmol), toluene (8 mL) and distilled water (2 mL). The resulting mixture was degassed by bubbling nitrogen for 15 minutes. Then the catalysts Pd(OAc)<sub>2</sub> (8 mg, 0.037 mmol), S-Phos (31 mg, 0.075 mmol), the base K<sub>3</sub>PO<sub>4</sub> (669 mg, 3 mmol) and Aliquat 3,3,6 (4 drops) were added and the resulting dark solution was heated at 100°C for 16hs, then it was allowed to reach room temperature. The solvent was evaporated under reduced pressure. The residue was diluted with NaHCO<sub>3</sub> aq 10% (30 mL) and extracted with dichlorometane (3 x 30 mL). The organic extracts were collected, dried over anhydrous Na<sub>2</sub>SO<sub>4</sub> and filtered off. The solvent was removed under reduced pressure and the crude material was purified by column chromatography on silica gel, eluting with a solvent mixture of AcOEt:DCM:Et<sub>3</sub>N in volumetric ratio 50:49:1. A red solid (134 mg) was isolated with a yield of 41%. Mp: the product starts decomposing at 160 °C. <sup>1</sup>H NMR (400 MHz, CDCl<sub>3</sub>) δ 8.53 – 8.49 (m, 2H), 7.22 (dd, J = 5.1, 1.1 Hz, 1H), 7.17 (dd, J = 3.6, 1.1 Hz, 1H), 7.12 (d, J = 5.9 Hz, 2H), 7.09 – 6.95 (m, 6H), 6.64 (d, J = 3.6 Hz, 1H), 3.13 (t, J = 7.7 Hz, 2H), 2.99 (t, J = 7.6 Hz, 2H). <sup>13</sup>C NMR (95 MHz, CDCl<sub>3</sub>) δ 147.2, 137.0, 136.3, 135.7, 135.5, 127.9, 127.8, 125.9, 124.7, 124.6, 124.5, 124.4, 124.3, 124.2, 124.19, 124.0, 123.7, 123.7, 123.4, 37.2, 29.7. HRMS (ESI-TOF) m/z: [M+H]<sup>+</sup> Calc for C<sub>23</sub>H<sub>17</sub>NS<sub>4</sub> 436.0317, Found 436.0276

#### Synthesis of 3a-d complexes

**General** All the solvents and reagents were used as received from Aldrich, Fluka, TCI and VWR without further purification. K<sub>2</sub>PtCl<sub>4</sub> was purchased from Precious Metal Online (PMO). PtCl<sub>2</sub>(DMSO)<sub>2</sub>, was prepared by following already reported synthetic procedures. All the synthesis and characterization of the ligands and the complexes are described below. Nucler

Magnetic Resonance (NMR) spectra were recorded on a Bruker Avance 400 spectrometer. The  $^1\text{H}$  NMR chemical shifts ( $\delta$ ) are given in ppm and referred to residual protons on the corresponding deuterated solvent. All deuterated solvents were used as received without any further purification. Electro-Spray Ionisation Mass Spectrometry (ESI-MS) experiments were performed on a Bruker Daltonics microTOF spectrometer (Bruker Daltonik GmbH, Bremen, Germany) equipped with an orthogonal (ESI) interface. Calibration was performed using Tuning mix (Agilent Technologies). Sample solutions were introduced into the spectrometer source with a syringe pump (Harvard type 55 1111: Harvard Apparatus Inc., South Natick, MA, USA) with a flow rate of  $5\ \mu\text{L}\cdot\text{min}^{-1}$ .

### Synthetic methods for complexes 3a-d

The pyridine-based ligands (1 eq), the tridentate ligand (1 eq) and the platinum precursor  $\text{Pt}[\text{Cl}_2(\text{dms})_2]$  (1 eq) are mixed and dissolved in ethyleneglycol dimethylether. Diisopropyl ethyl amine (DIPEA) is then added (2.5 eq) and the reaction mixture is stirred for 24 hours at  $110\ ^\circ\text{C}$ . Water is added then to the crude and the products precipitate and are isolated after filtration. The products are obtained as yellow (3a, 3e, 3f, 3g), orange (3b, 3d) and red (3d) powders.

**3a:**  $^1\text{H}$  NMR (400 MHz,  $\text{CDCl}_3$ )  $\delta$ : 9.57 (d, 2H), 8.02 (t, 1H), 7.79 (d, 2H), 7.73 (t, 3H), 7.66 (d, 1H), 7.27 (t, 1H).  $^{13}\text{C}$  NMR (100 MHz,  $\text{CDCl}_3$ )  $\delta$ : 153.29, 148.86, 142.95, 142.30, 138.75, 130.45, 129.36, 128.15, 118.18, 118.13.  $^{19}\text{F}\{^1\text{H}\}$  NMR (400 MHz,  $\text{CDCl}_3$ )  $\delta$ : -64.20. HR-ESI-MS (m/z):  $[\text{M}]^+\text{calcd}$ : 703.0301; found: 704.0279. Yield (75 %).

**3b:**  $^1\text{H}$  NMR (400 MHz,  $\text{CDCl}_3$ )  $\delta$ : 9.65 (d, 2H), 8.11 (t, 1H), 7.92 (d, 2H), 7.76 (d, 2H), 7.67 (d, 1H), 7.24 (d, 1H), 7.19 (d, 1H), 6.81 (d, 1H), 2.88 (t, 2H), 1.75 (m, 2H), 1.34 (m, 10H), 0.94 (m, 3H).  $^{13}\text{C}$  NMR (100 MHz,  $\text{CDCl}_3$ )  $\delta$ : 153.64, 153.44, 149.25, 143.5, 142.79, 136.82, 136.07, 135.87, 135.59, 134.97, 134.59, 133.39, 129.03, 125.27, 125.2, 124.58, 121.69, 121.2, 119.48, 118.18, 118.09, 31.78, 31.46, 29.64, 22.58.  $^{19}\text{F}\{^1\text{H}\}$  NMR (400 MHz,  $\text{CDCl}_3$ )  $\delta$ : -64.23. HR-ESI-MS (m/z):  $[\text{M}]^+\text{calcd}$ : 897.1430; found: 898.1472. Yield (55 %).

**3c:**  $^1\text{H}$  NMR (400 MHz,  $\text{CDCl}_3$ )  $\delta$ : 9.66 (d, 2H), 8.08 (t, 1H), 7.91 (d, 2H), 7.76 (d, 2H), 7.68 (d, 1H), 7.54 (s, 1H), 7.47 (m, 2H), 7.16 (d, 2H), 7.08 (t, 1H).  $^{13}\text{C}$  NMR (100 MHz, DMSO)  $\delta$ : 182.08, 181.85, 153.55, 150.91, 143.04, 140.56, 138.27, 136.94, 128.89, 128.08, 126.68, 126.42, 126.31, 126.05, 125.56, 125.05, 122.19, 119.76, 118.88.  $^{19}\text{F}\{^1\text{H}\}$  NMR (400 MHz,  $\text{CDCl}_3$ )  $\delta$ : -64.24. HR-ESI-MS (m/z):  $[\text{M}]^+\text{calcd}$ : 869.0101; found: 867.7304. Yield (40 %).

**3d:**  $^1\text{H}$  NMR (400 MHz,  $\text{CDCl}_3$ )  $\delta$ : 9.56 (d, 2H), 8.06 (t, 1H), 7.84 (d, 2H), 7.44 (d, 2H), 7.23 (d, 1H), 6.99 (dd, 1H), 6.86 (d, 1H), 3.33 (t, 2H), 3.20 (t, 2H).  $^{13}\text{C}$  NMR (100 MHz,  $\text{CDCl}_3$ )  $\delta$ : 163.17, 154.69, 152.85, 142.84, 142.17, 141.24, 127.08, 126.50, 125.04, 124.26, 117.98, 37.15, 29.64.  $^{19}\text{F}\{^1\text{H}\}$  NMR (400 MHz,  $\text{CDCl}_3$ )  $\delta$ : -64.29. HR-ESI-MS (m/z):  $[\text{M}]^+\text{calcd}$ : 731.0614; found: 730.956. Yield (65 %).

### Photophysical measurements

All solvents used for spectroscopical characterization were spectrometric grade and purchased by VWR. Absorption spectra were measured on a Shimadzu UV-3600 spectrophotometer double-beam UV-VIS-NIR spectrometer and baseline corrected. Steady-state emission spectra were recorded on a Horiba Jobin-Yvon IBH FL-322 Fluorolog 3 spectrometer equipped with a 450 W xenon arc lamp, double-grating excitation, and emission monochromators ( $2.1\ \text{nm}\ \text{mm}^{-1}$  of dispersion;  $1200\ \text{grooves}\ \text{mm}^{-1}$ ) and a TBX-04 single photon-counting detector. Emission

and excitation spectra were corrected for source intensity (lamp and grating) and emission spectral response (detector and grating) by standard correction curves. Time-resolved measurements were performed using the time-correlated single-photon-counting (TCSPC) option on the Fluorolog 3. NanoLEDs (402 nm; fwhm <200 ns) with repetition rates between 10 kHz and 1 MHz was used to excite the sample. The excitation sources were mounted directly on the sample chamber at 90° to a double-grating emission monochromator (2.1 nm mm<sup>-1</sup> of dispersion; 1200 grooves mm<sup>-1</sup>) and collected by a TBX-04 single-photon-counting detector. The photons collected at the detector are correlated by a time-to-amplitude converter to the excitation pulse. Signals were collected using an IBH DataStation Hub photon-counting module and data analysis was performed using the commercially available DAS6 software (Horiba Jobin-Yvon IBH). The quality of the fit was assessed by minimizing the reduced  $\chi^2$  function and by visual inspection of the weighted residuals. For multi-exponential decays, the intensity, namely  $I(t)$ , has been assumed to decay as the sum of individual single exponential decays as by the following equation:

$$I(t) = \sum_{i=1}^n a_i e^{-\frac{t}{\tau_i}}$$

where  $\tau_i$  are the decay times and  $a_i$  are the amplitude of the component at  $t = 0$ . The percentages to the pre-exponential factors,  $a_i$ , are listed upon normalization. The quantum yield measurements were performed by using an absolute photoluminescence quantum yield spectrometer Quantaurus C11347 (Hamamatsu, Japan) exciting the sample at  $\lambda_{exc} = 350$  and 400 nm. All solvents were spectrometric grade. The measurements were performed on samples at 50  $\mu$ M concentration.

Solid state measurements. Steady-state measurements on solid state samples were recorded on a Horiba Jobin-Yvon IBH FL-322 Fluorolog 3 spectrometer as described before. Time-resolved measurements were performed using the time-correlated single-photon-counting option on the Fluorolog 3. NanoLEDs (402 nm; fwhm <200 ns) with repetition rates between 10 kHz and 1 MHz was used to excite the sample. The excitation sources were mounted directly on the sample chamber at 90° to a double-grating emission monochromator (2.1 nm mm<sup>-1</sup> of dispersion; 1200 grooves mm<sup>-1</sup>) and collected by a TBX-04 single-photon-counting detector. The photons collected at the detector are correlated by a time-to-amplitude converter to the excitation pulse. Signals were collected using an IBH DataStation Hub photon-counting module and data analysis was performed using the commercially available DAS6 software (Horiba Jobin-Yvon IBH).

## DFT calculations

The optimized geometries of the singlet ground state of the presented Pt complexes were verified to be true minima by frequency analysis revealing no imaginary frequencies. The utilizing the parameter-free hybrid functional Perdew-Burke-Ernzerhof PBE0<sup>1-3</sup> was employed with the standard valence basis set 6-31G(d,p) for C,H,N,S and F.4 The Stuttgart-Dresden effective core potential<sup>5,6</sup> along with its corresponding basis set was employed for Pt. To simulate the measured absorption UV-vis spectrum, the lowest lying 50 vertical singlet electronic excitation energies were calculated using time-dependent DFT (TD-DFT) at the S0 optimized geometry. The TD-DFT calculations were performed in solution using dichloromethane as solvent with the polarization continuum model and with the same functional and basis set as in the optimizations. All these calculations were performed with the Gaussian09 program package.<sup>7</sup> The analysis of the EDDM calculations were performed by



GaussSum2.2.<sup>8</sup> Electron-density difference maps (density isovalue = 0.001) and Kohn–Sham orbitals (MO isovalue = 0.04) were visualized by Gauss-View5.0.8.<sup>7</sup>

### Scanning electron microscopy

SEM images were recorded with a FEI Quanta FEG 250 instrument (FEI corporate, Hillsboro, Oregon, USA) with an acceleration voltage of 20 kV. The sample is prepared by drop-casting solutions of complexes onto a glass cover slip, subsequently sputter coated with Au (Emitech K575X peltier cooled) for 20 s at 60 mA prior to fixation on an Al support.

### Cyclic voltammetry

The electrochemical characterization of the Pt complexes herein reported has been performed in CH<sub>2</sub>Cl<sub>2</sub>/0.1 M tetra-butylammonium hexafluorophosphate (TBAPF<sub>6</sub>). The concentration of the complexes was 1 mM. Oxygen was removed by purging the CH<sub>2</sub>Cl<sub>2</sub> solution with high-purity Argon.

A typical three-electrode cell was employed, which was composed of a glassy carbon working electrode (3 mm diameter, 66-EE047 Cypress Systems), a platinum wire as counter, and a silver wire as quasi-reference (QRE) electrode. A CHI750C Electrochemical Workstation (CH Instruments, Inc., Austin, TX, USA) was used.

The potential of the reference electrode was calibrated after each measurement using Ferrocene/Ferrocenium (Fc/Fc<sup>+</sup>) redox couple as the internal standard. The formal potential of Fc/Fc<sup>+</sup> is 0.460V for CH<sub>2</sub>Cl<sub>2</sub> against the KCl saturated calomel electrode (SCE).

The GC electrodes were stored in ethanol, and before experiments were polished with a 0.05 μm diamond suspension (Metadi Supreme Diamond Suspension, Buehler) and ultrasonically rinsed with deionized water for 5 minutes and ethanol for 5 minutes. The electrodes were electrochemically activated in the background solution by means of several voltammetric cycles at 0.5 Vs<sup>-1</sup> between the anodic and cathodic solvent/electrolyte discharges.

The standard potentials were calculated as the average value between cathodic and anodic peak potentials, when the processes are reversible or quasi-reversible.

All the CVs were performed at 0.1 V/s.

### Powder X-ray diffraction (PXRD)

PXRD data were acquired using a Bruker D2-PHASER diffractometer using CuKα radiation (λ = 1.5418 Å) at 300W (30kV, 10mA) power with Ni Kβ-filter and equipped by a 0.1mm divergence slit and 1mm air scatter screen. The samples were manually grounded in an agate mortar, then deposited on a zero background silicon sample holder. All the measurements were performed in the Bragg-Brentano geometry, with 2θ values ranging from 5 to 40° with an exposure time of several seconds per step. All samples were measured at room temperature and room pressure. The crystal parameters were determined using TOfal Pattern Analysis Solution program (TOPAS) after refinement using the indexing method.

### SCLC

Indium Tin Oxide (ITO) coated glass was used as substrate. PEDOT:PSS was used as the hole injection electrode to extract hole mobility. The device structure is ITO/PEDOT:PSS/Active layer/MoO<sub>3</sub>/Ag. A 120 nm thick silver on top of a 7 nm thick Molybdenum trioxide (MoO<sub>3</sub>) layer were thermal evaporated as the top electrode for measuring the hole mobility. The top electrode surface ranged from 2.25x10<sup>-3</sup> mm<sup>2</sup> to 0.25 mm<sup>2</sup>.

The substrates were cleaned in acetone, isopropyl alcohol and deionized water at 45°C for 15 minutes, respectively; then under ultra-violet ozone for 30 minutes. PEDOT:PSS was spin-coated on the top of ITO layer and then dried at 140°C for 30 minutes. Then devices were fabricated by spin coating (500 rpm, 120 seconds) 200 μl of complex **3a** and by drop casting 80

$\mu$ l of complexes **3b-d** in ODCB. [3a-d] = 0.01 M. Devices were then measured in glovebox by the Keithley 4200 semiconductor characterization system. SCLC mobility values were calculated according to the Mott-Gurney's law following the equation:

$$J = \frac{9}{8} \epsilon \epsilon_0 \mu_h \frac{V^2}{L^3}$$

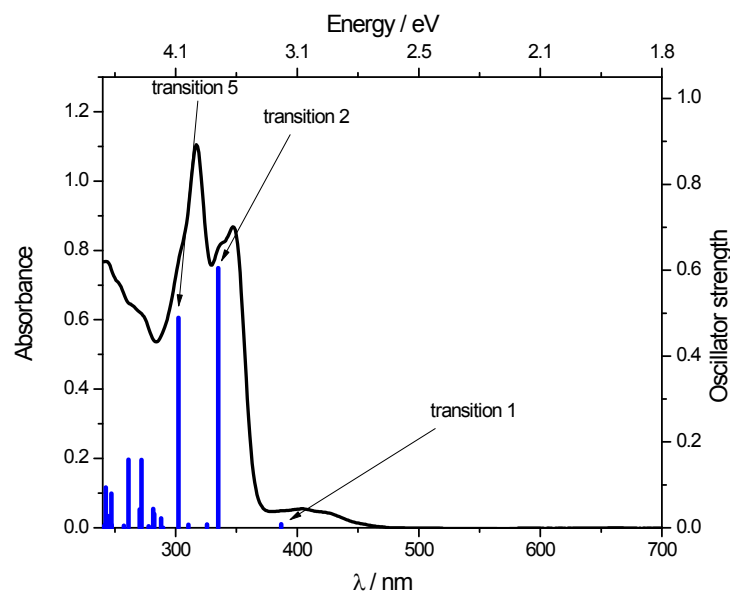
Where J is the current density,  $\epsilon_0$  is the vacuum permittivity while  $\epsilon$  is the dye dielectric constant,  $\mu$  is the mobility, V is the voltage and L is the thickness of the active layer.

$$\mu_h = \frac{8 \cdot a \cdot L^3}{9 \cdot \epsilon \epsilon_0 \cdot S}$$

### Atomic Force Microscopy (AFM)

AFM measurements for all the Pt(II) complex samples were performed under ambient conditions using a Veeco diMultimode V system equipped with a Nanoscope V controller. SCM-PIC tips with a nominal force constant of 0.2 N m<sup>-1</sup> and a nominal tip radius of 20 nm were used in contact mode. All samples for the AFM analysis were prepared by drop-casting on Si-SiO<sub>2</sub> substrates and allowed to dry completely before the analysis. For the sake of clarity and ease of comprehension, the results of the morphological studies are displayed in 3D images obtained by superimposing the characteristic height and deflection error of each sample. Indeed, the aforementioned approach allows a more illustrative way to denote the different roughness values of the investigated supramolecular Pt-based assemblies summarized in Table S17. In particular, the available data in the Table S17 describe the roughness R<sub>q</sub> for each assembly, where R<sub>q</sub> is the root mean square average of the deviation taken from the mean image data plane."

## Supporting figures and tables

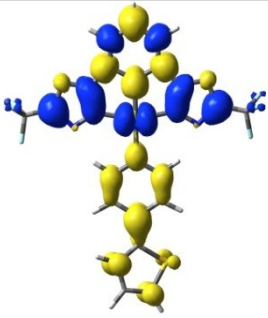
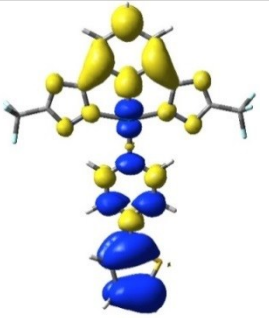
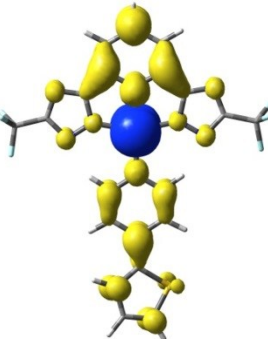
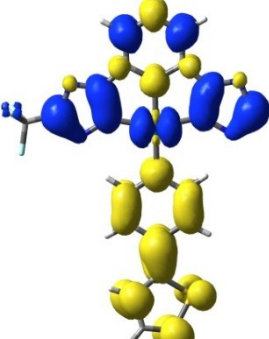
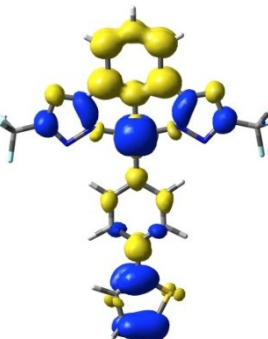

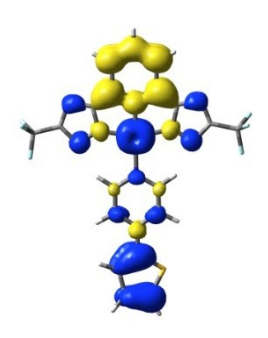
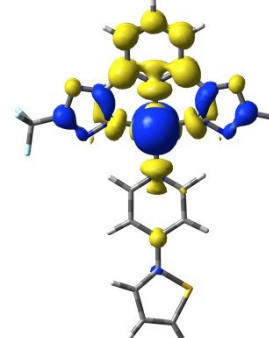


**Figure S1.** Measured (black, solid line) and calculated (blue bars) UV-Vis absorption spectra of compound **3a**.

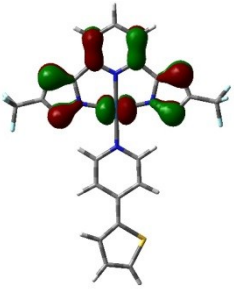
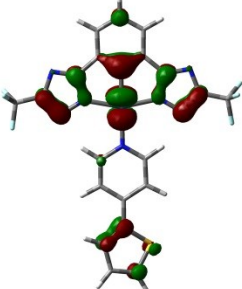
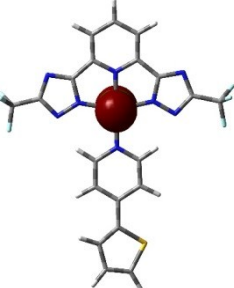
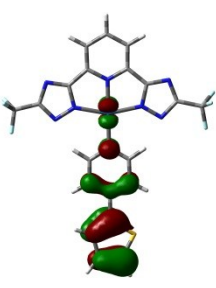
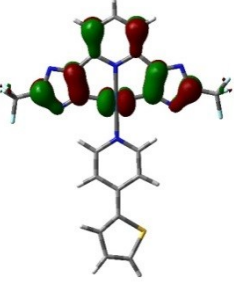
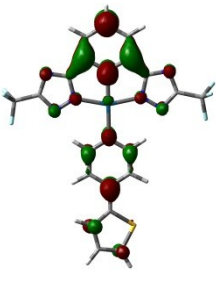
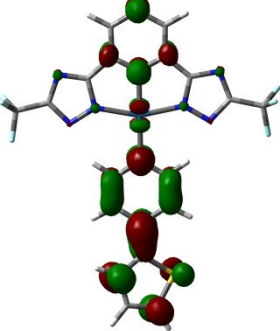
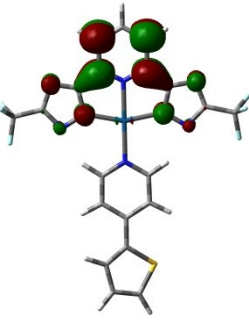
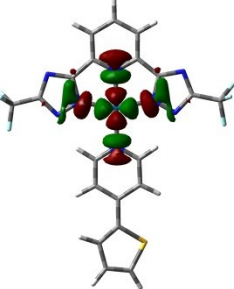
**Table S1.** Calculated electronic singlet transitions for compound **3a**, based on TD-DFT:

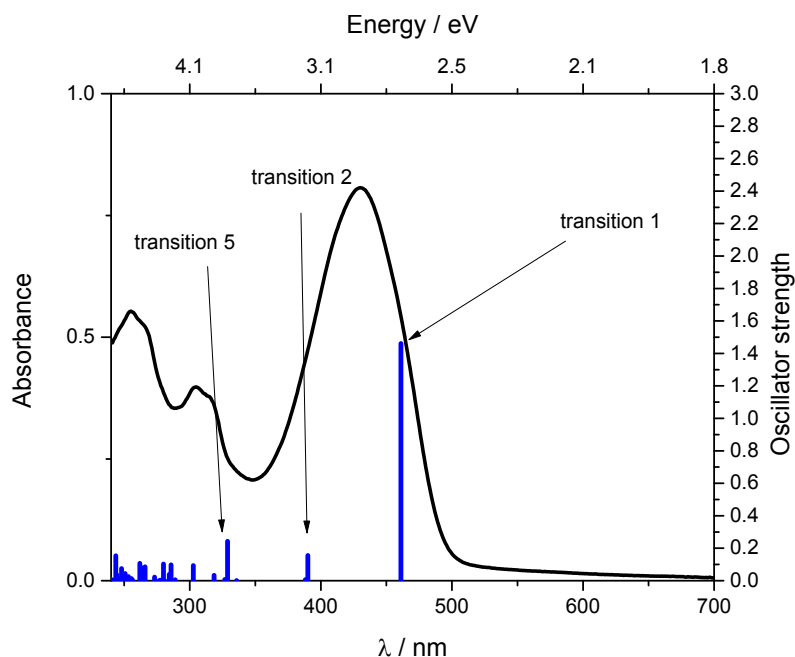
No.	$\lambda$ (nm)	f	Major contributions	Minor contributions
1	386	0.0085	HOMO→LUMO (91%)	HOMO→L+1 (8%)
2	335	0.605	H-1→LUMO (90%)	H-4→LUMO (5%)
3	325	0.008	H-2→LUMO (93%)	H-2→L+1 (7%)
4	310	0.0069	HOMO→L+1 (90%)	HOMO→LUMO (8%)
5	302	0.4889	H-2→L+4 (11%), H-1→L+1 (35%), HOMO→L+2 (41%)	H-4→LUMO (7%)
6	288	0.0001	H-5→L+4 (11%), HOMO→L+4 (85%)	
7	287	0.0217	H-1→L+1 (60%), HOMO→L+2 (26%)	H-4→LUMO (5%), H-1→LUMO (5%)
8	282	0.0323	H-5→LUMO (41%), H-4→L+2 (11%), H-1→L+2 (42%)	H-5→L+1 (3%)
9	281	0.0442	H-4→LUMO (24%), H-2→L+4 (45%), HOMO→L+2 (22%)	

**Table S2.** Electron-density-difference maps representing the singlet transitions calculated for compound **3a**. The blue isosurfaces represent the depletion of electron density and the yellow isosurfaces represent the accumulation of electron density during an electronic transition. (isovalue=0.001)

transition 1			transition 2
transition 3			transition 4
transition 5			transition 7
transition 8			transition 9

**Table S3.** Kohn-Sham plots of the molecular orbitals (isovalue=0.04) involved of the electronic transitions displayed above as EDDM plots above of **3a**:

HOMO-5			HOMO-4
HOMO-2			HOMO-1
HOMO			LUMO
LUMO+1			LUMO+2
LUMO+3			

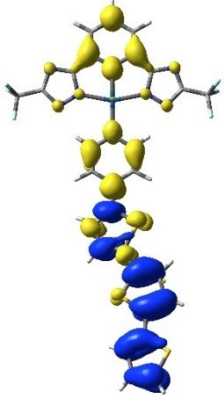
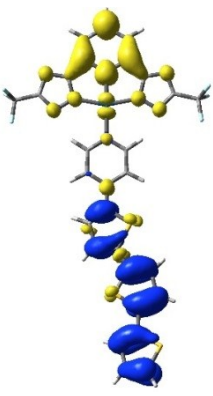
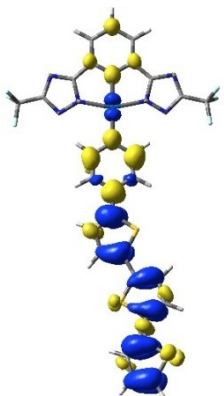
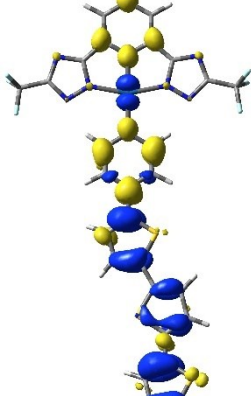
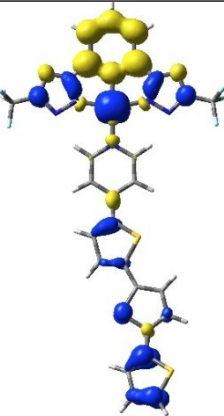


**Figure S2.** Measured (black, solid line) and calculated (blue bars) UV-Vis absorption spectra of compound **3b**.

**Table S4.** Calculated electronic singlet transitions for compound **3 b**, based on TD-DFT:

No.	$\lambda$ (nm)	f	Major contribs	Minor contribs
1	461	1.4612	HOMO->LUMO (94%)	HOMO->L+1 (5%)
2	390	0.1553	HOMO->L+1 (94%)	HOMO->LUMO (5%)
3	388	0.0072	H-1->LUMO (66%), H-1->L+1 (32%)	
4	336	0.0005	HOMO->L+2 (99%)	
5	329	0.2432	H-2->LUMO (37%), HOMO->L+3 (56%)	
6	328	0.0063	H-1->LUMO (31%), H-1->L+1 (63%)	H-1->L+3 (3%)
7	327	0.0078	H-3->LUMO (68%), H-3->L+1 (31%)	
8	319	0.0328	H-2->LUMO (47%), HOMO->L+3 (38%)	H-6->LUMO (6%), H-5->L+1 (2%)
9	303	0.0935	H-2->L+1 (22%), H-1->L+2 (39%)	H-6->LUMO (5%), H-6->L+1 (4%), H-5->LUMO (6%), H-3->L+5 (9%), H-2->LUMO (6%)

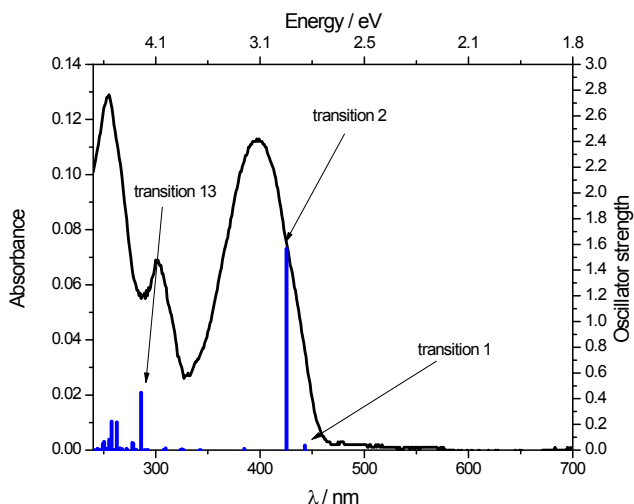
**Table S5.** Electron-density-difference maps representing the singlet transitions calculated for compound **b**. The blue isosurfaces represent the depletion of electron density and the yellow isosurfaces represent the accumulation of electron density during an electronic transition. (isovalue=0.001)

transition 1			transition 2
transition 5			transition 8
transition 9			

**Table S6.** Kohn-Sham plots of the molecular orbitals (isovalue=0.04) involved of the electronic transitions displayed above as EDDM plots above of **3b**

HOMO-5			HOMO-3
HOMO-2			HOMO-1
HOMO			LUMO
LUMO+1			LUMO+2
LUMO+3			LUMO+5



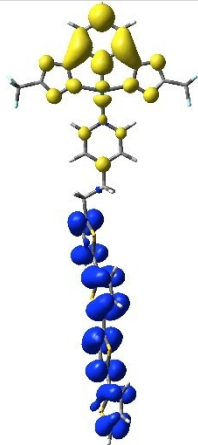
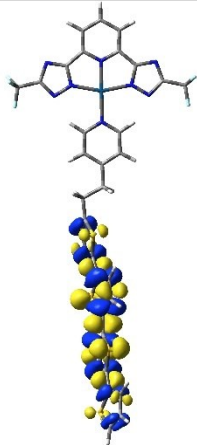
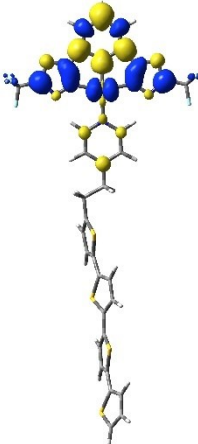
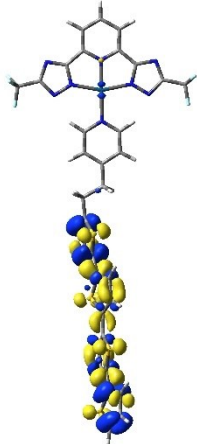
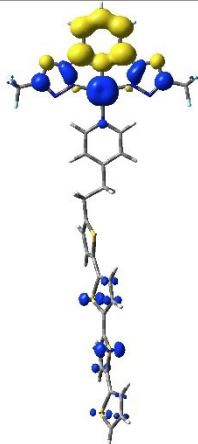


**Figure S3.** Measured (black, solid line) and calculated (blue bars) UV-Vis absorption spectra of compound **3c**.

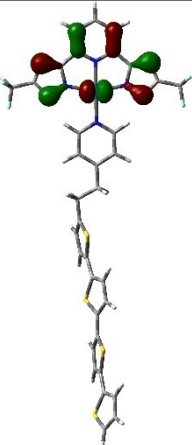
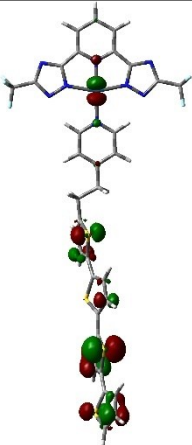
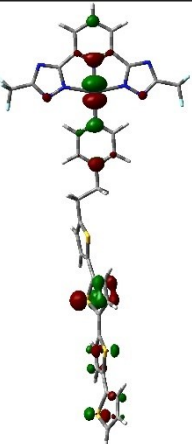
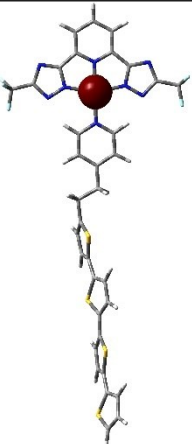
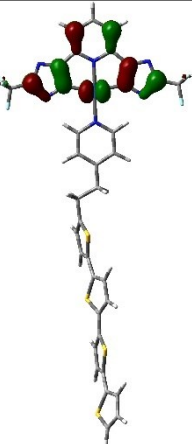
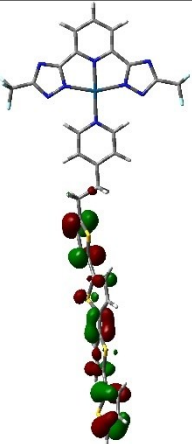
**Table S7.** Calculated electronic singlet transitions for compound **3c**, based on TD-DFT

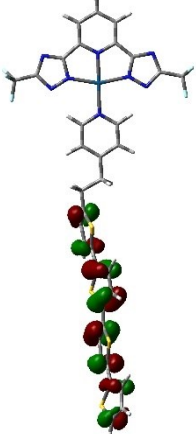
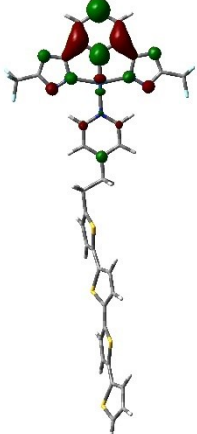
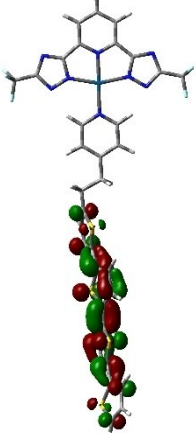
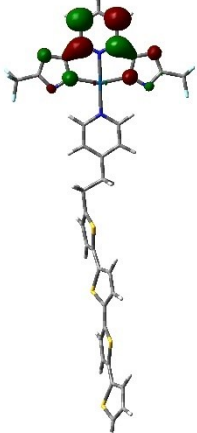
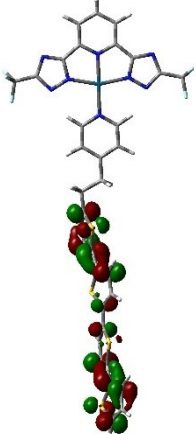
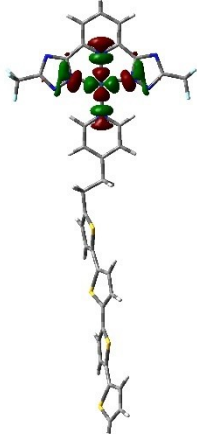
No.	$\lambda$ (nm)	f	Major contribs	Minor contribs
1	443	0.0364	HOMO→LUMO (98%)	
2	425	1.5651	HOMO→L+1 (98%)	
3	385	0.0095	H-2→LUMO (98%)	
4	360	0	HOMO→L+2 (100%)	
5	342	0.0002	HOMO→L+3 (95%)	
6	326	0.0006	H-1→LUMO (49%), H-1→L+1 (15%), HOMO→L+4 (26%)	H-5→LUMO (8%)
7	325	0.007	H-5→LUMO (86%)	H-1→L+1 (4%), HOMO→L+4 (7%)
8	324	0.0016	H-1→LUMO (48%), H-1→L+1 (14%), HOMO→L+4 (31%)	H-5→LUMO (3%), HOMO→L+3 (3%)
9	309	0.0139	H-1→L+1 (61%), HOMO→L+4 (31%)	H-6→LUMO (3%)
10	307	0.0025	H-7→LUMO (13%), H-6→LUMO (36%), H-2→L+2 (32%)	H-8→LUMO (2%), H-5→L+6 (7%), H-1→L+1 (4%), HOMO→L+4 (2%)
11	292	0.0002	HOMO→L+5 (98%)	
12	289	0.0001	H-10→L+6 (11%), H-2→L+6 (85%)	
13	286	0.4457	H-6→LUMO (25%), H-2→L+2 (52%)	H-10→L+2 (3%), H-7→LUMO (9%), H-5→L+6 (2%)

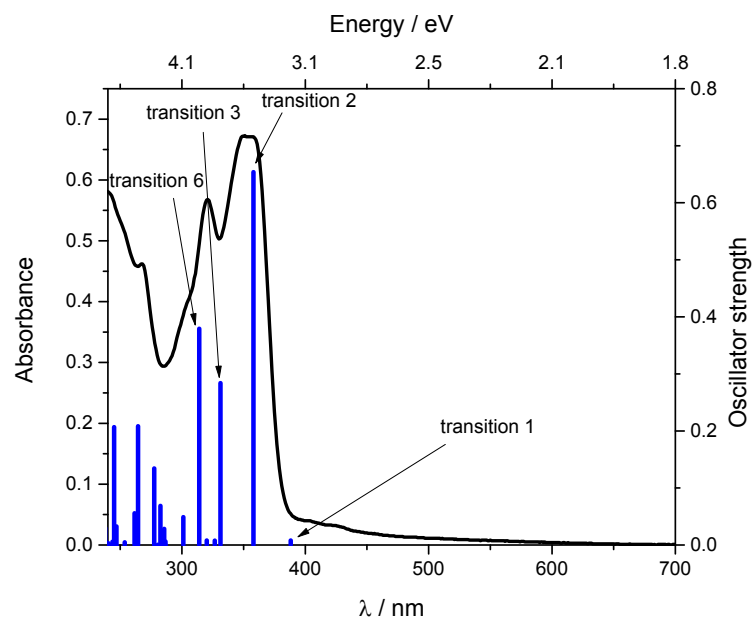
**Table S8.** Electron-density-difference maps representing the singlet transitions calculated for compound **3c**. The blue isosurfaces represent the depletion of electron density and the yellow isosurfaces represent the accumulation of electron density during an electronic transition. (isovalue=0.001)

transition 1			transition 2
transition 3			transition 9
transition 13			

**Table S9.** Kohn-Sham plots of the molecular orbitals (isovalue=0.04) involved of the electronic transitions displayed above as EDDM plots above of **3c**.

HOMO-10	 Molecular orbital plot for HOMO-10. The structure shows a complex, multi-ring system with a central nitrogen atom. The orbital is localized on the top part of the molecule, with several lobes of positive (red) and negative (green) phase.
HOMO-7	 Molecular orbital plot for HOMO-7. The structure shows a complex, multi-ring system with a central nitrogen atom. The orbital is localized on the top part of the molecule, with several lobes of positive (red) and negative (green) phase.
HOMO-6	 Molecular orbital plot for HOMO-6. The structure shows a complex, multi-ring system with a central nitrogen atom. The orbital is localized on the top part of the molecule, with several lobes of positive (red) and negative (green) phase.
HOMO-5	 Molecular orbital plot for HOMO-5. The structure shows a complex, multi-ring system with a central nitrogen atom. The orbital is localized on the top part of the molecule, with several lobes of positive (red) and negative (green) phase.
HOMO-2	 Molecular orbital plot for HOMO-2. The structure shows a complex, multi-ring system with a central nitrogen atom. The orbital is localized on the top part of the molecule, with several lobes of positive (red) and negative (green) phase.
HOMO-1	 Molecular orbital plot for HOMO-1. The structure shows a complex, multi-ring system with a central nitrogen atom. The orbital is localized on the bottom part of the molecule, with several lobes of positive (red) and negative (green) phase.

HOMO			LUMO
LUMO+1			LUMO+2
LUMO+4			LUMO+6

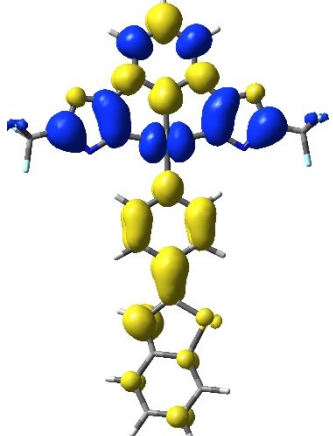
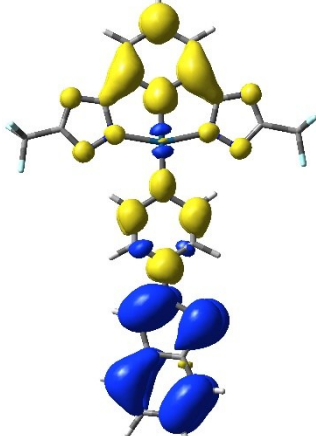
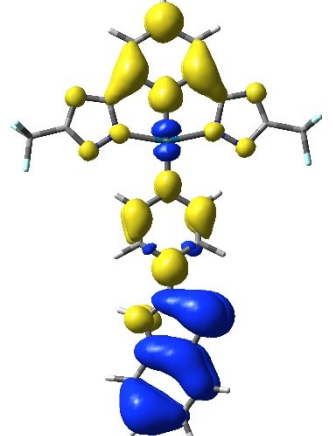
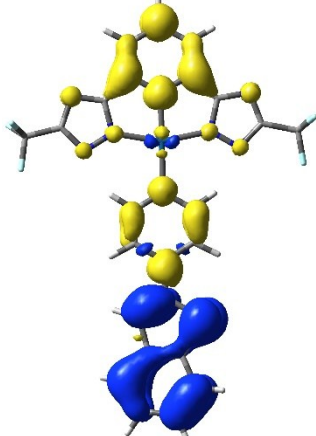
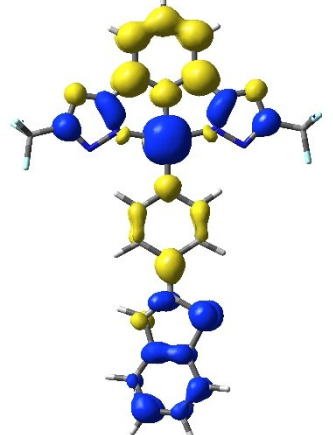


**Figure S4.** Measured (black, solid line) and calculated (blue bars) UV-Vis absorption spectra of compound **3d**

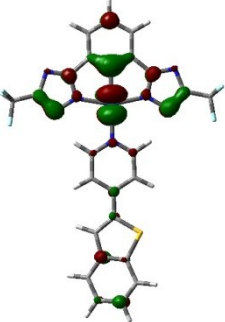
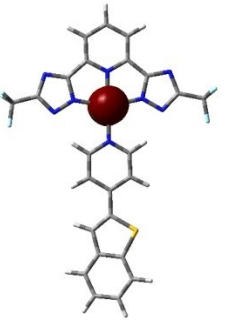
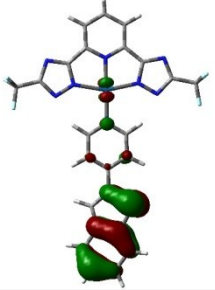
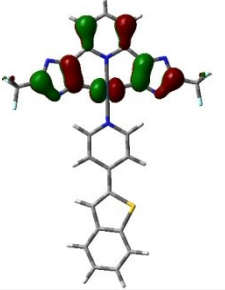
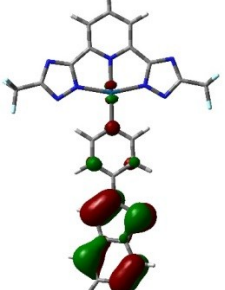
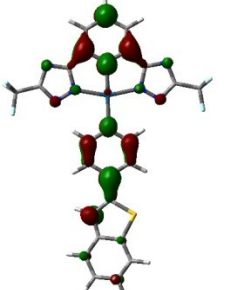
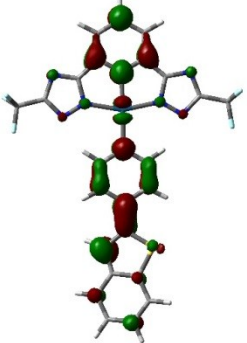
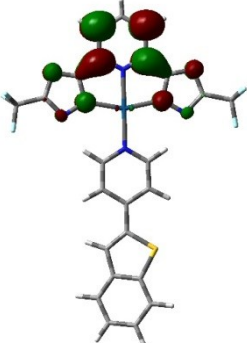
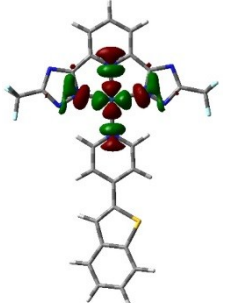
**Table S10.** Calculated electronic singlet transitions for compound **3d** based on TD-DFT

No.	$\lambda$ (nm)	f	Major contribs	Minor contribs
1	388	0.008	H-1->LUMO (84%), H-1->L+1 (14%)	
2	358	0.654	HOMO->LUMO (92%)	HOMO->L+1 (5%)
3	331	0.284	H-2->LUMO (79%)	H-4->LUMO (3%), H-2->L+1 (9%), HOMO->L+1 (6%)
4	327	0.008	H-3->LUMO (87%), H-3->L+1 (13%)	
5	320	0.008	H-1->LUMO (14%), H-1->L+1 (83%)	
6	314	0.379	HOMO->L+1 (77%)	H-2->LUMO (5%), H-2->L+1 (4%), H-1->L+2 (6%), HOMO->LUMO (3%)
7	301	0.049	H-4->LUMO (22%), H-2->L+1 (14%), H-1->L+2 (36%), HOMO->L+1 (11%)	H-4->L+1 (3%), H-3->L+4 (8%), HOMO->LUMO (3%)
8	289	0.000	H-5->L+4 (11%), H-1->L+4 (85%)	
9	287	0.006	H-5->LUMO (11%), HOMO->L+2 (69%)	H-5->L+1 (2%), H-4->L+2 (7%), H-3->L+1 (3%), H-2->L+2 (4%)
10	287	0.000	H-3->LUMO (12%), H-3->L+1 (82%)	HOMO->L+2 (2%)
11	286	0.028	H-2->L+1 (43%), H-1->L+2 (35%)	H-4->LUMO (8%), H-2->LUMO (5%)
12	283	0.069	H-4->LUMO (48%), H-2->L+1 (24%)	H-3->L+4 (7%), H-2->LUMO (8%), H-1->L+2 (9%)
13	280	0.000	H-4->LUMO (13%), H-3->L+4 (79%)	H-1->L+2 (4%)
14	278	0.134	H-5->LUMO (68%), HOMO->L+2 (21%)	H-5->L+1 (6%), H-4->L+2 (3%)

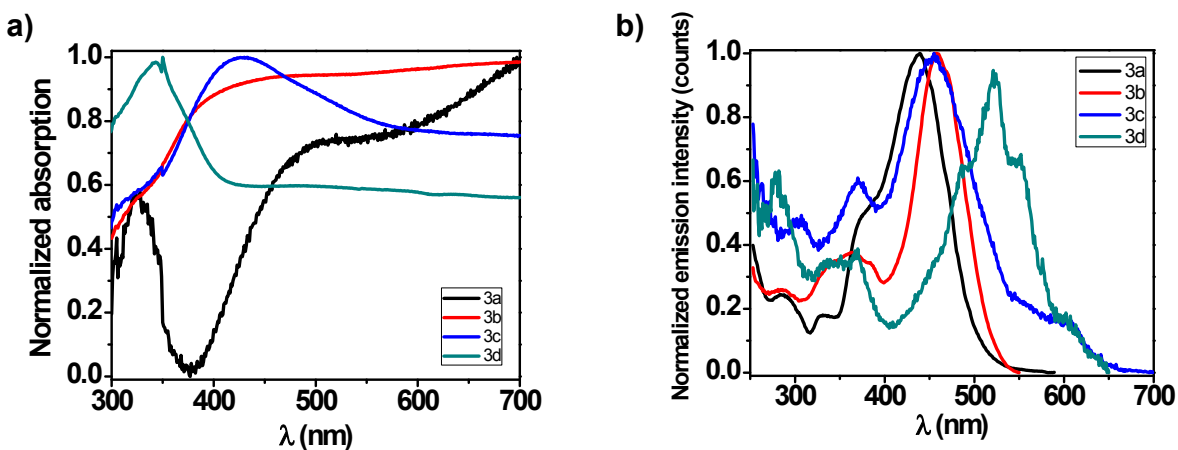
**Table S11.** Electron-density-difference maps representing the singlet transitions calculated for compound **3d**. The blue isosurfaces represent the depletion of electron density and the yellow isosurfaces represent the accumulation of electron density during an electronic transition. (isovalue=0.001)

transition 1			transition 2
transition 3			transition 6
transition 7			

**Table S12.** Kohn-Sham plots of the molecular orbitals (isovalue=0.04) involved of the electronic transitions displayed above as EDDM plots above of 3d.

HOMO-4			HOMO-3
HOMO-2			HOMO-1
HOMO			LUMO
LUMO+1			LUMO+2
LUMO+4			

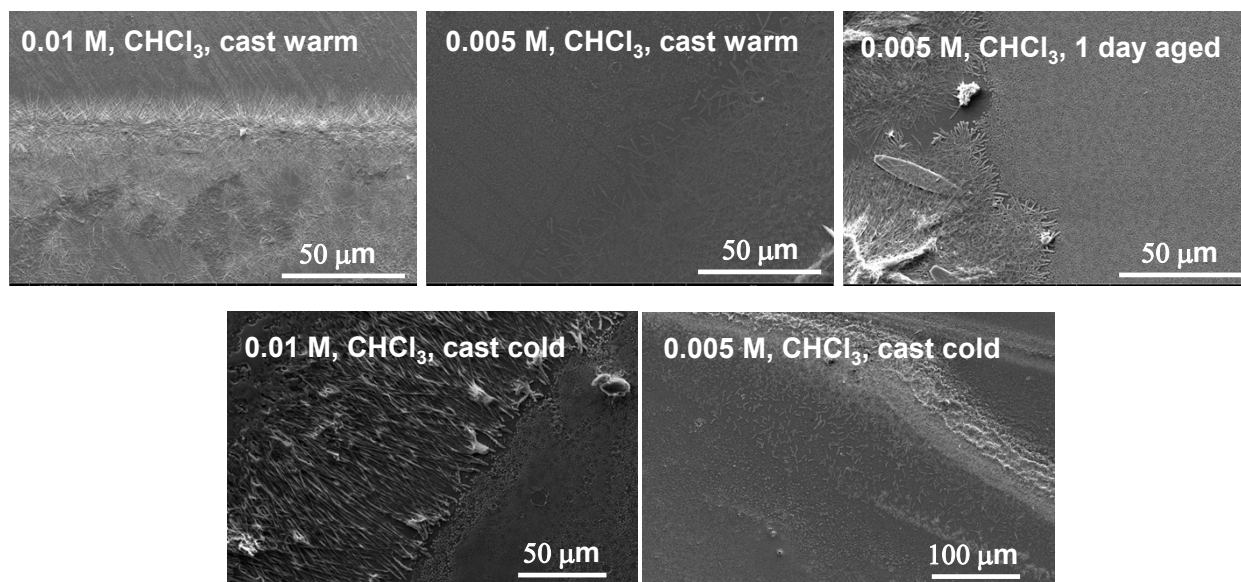




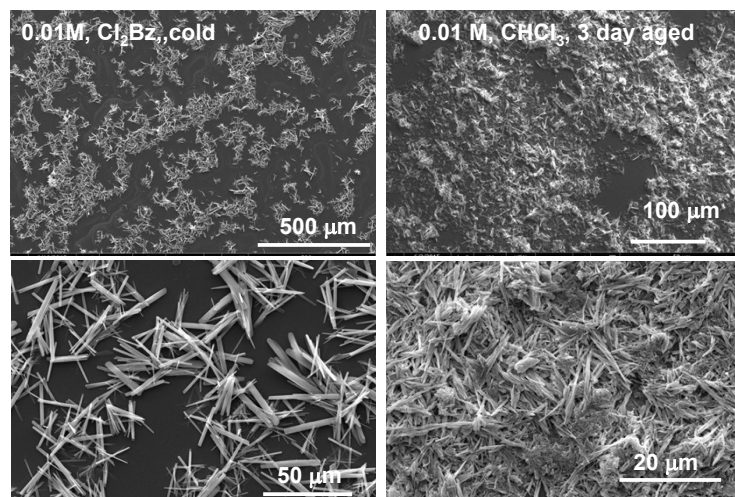
**Figure S5.** a) Thin film absorption spectra of complexes 3a-d. b) Excitation spectra of complexes **3a-d** in  $\text{CH}_2\text{Cl}_2$ ,  $[\mathbf{3a-d}] = 1 \times 10^{-5}$  M.

**Table S13:** Photophysical data of complexes **3a-d**.

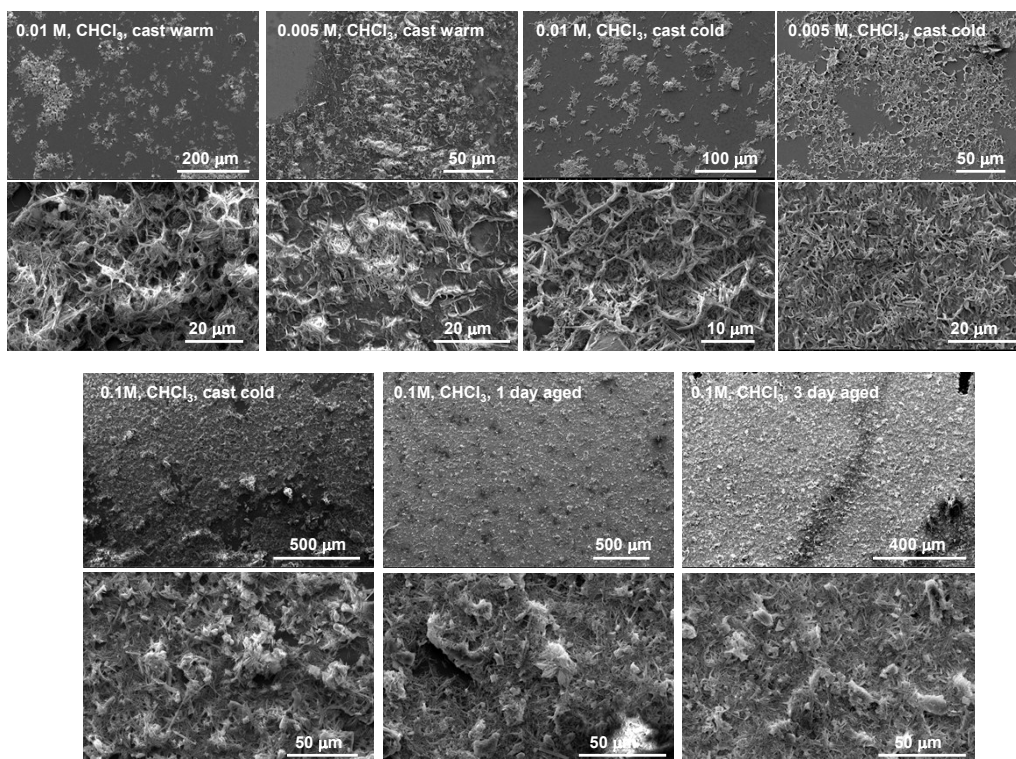
Complex	DCM solution, $[5 \times 10^{-5}\text{M}]$				Solid (powder)		
	$\lambda_{\text{abs}}$ , ( $\text{e} \cdot 10^{-4}$ ) [nm, $\text{M}^{-1} \cdot \text{cm}^{-1}$ ]	$\lambda_{\text{max}}$ [nm]	$\tau$ [ns]	PLQY (%)	$\lambda_{\text{em}}$ [nm]	$\tau$ [ns]	PLQY (%)
<b>3a</b>	246(1.51), 317(2.21), 347(1.73), 403(0.11)	525	0.8(77%), 2.6(20%)	1	598	463(37%), 182(55%), 54(8%)	3
<b>3b</b>	256(1.11), 304(0.79) 430 (1.62)	520	6.9(52%), 22(38%), 1.2(9%)	12	578	930(88%), 136(12%)	12
<b>3c</b>	254(0.26), 302(0.14), 397(0.23)	457, 487, 522	3(78%), 1.19(22%)	1.5	569, 611	495(80%), 147(20%)	1
<b>3d</b>	267(0.92), 320(1.13), 354(1.34), 418(0.07)	466, 498, 530, 595	7(61%), 0.82(7%), 3.8(32%)	1	461, 491, 557	955(77%), 156(21%), 10(2%)	1.5



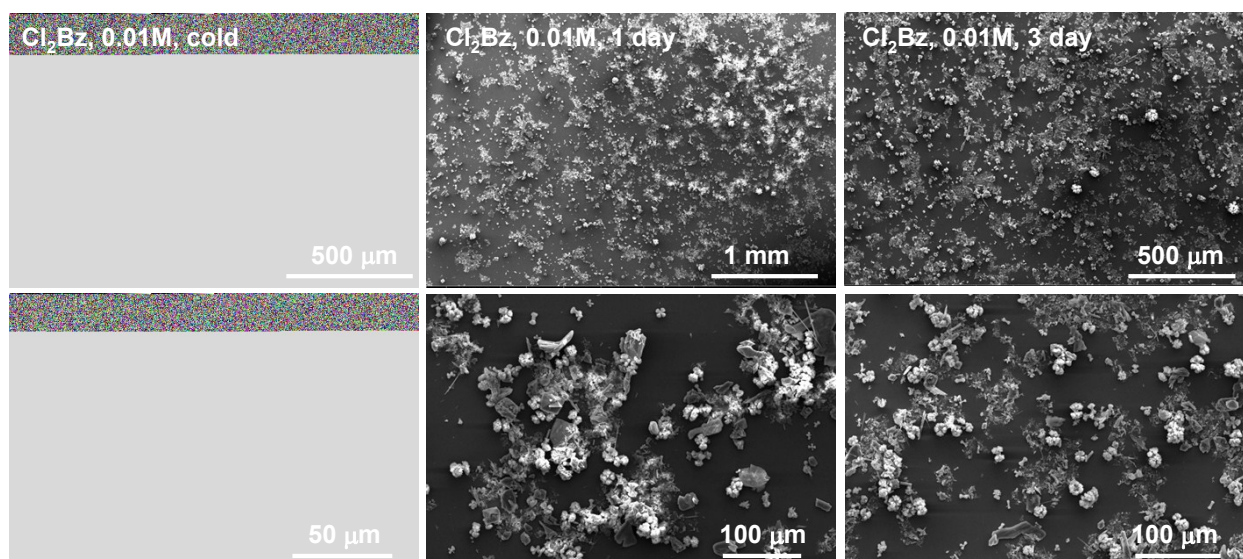
**Figure S6.** SEM images of films prepared with  $\text{CHCl}_3$  solutions of complex **3a** at different concentrations and casting conditions



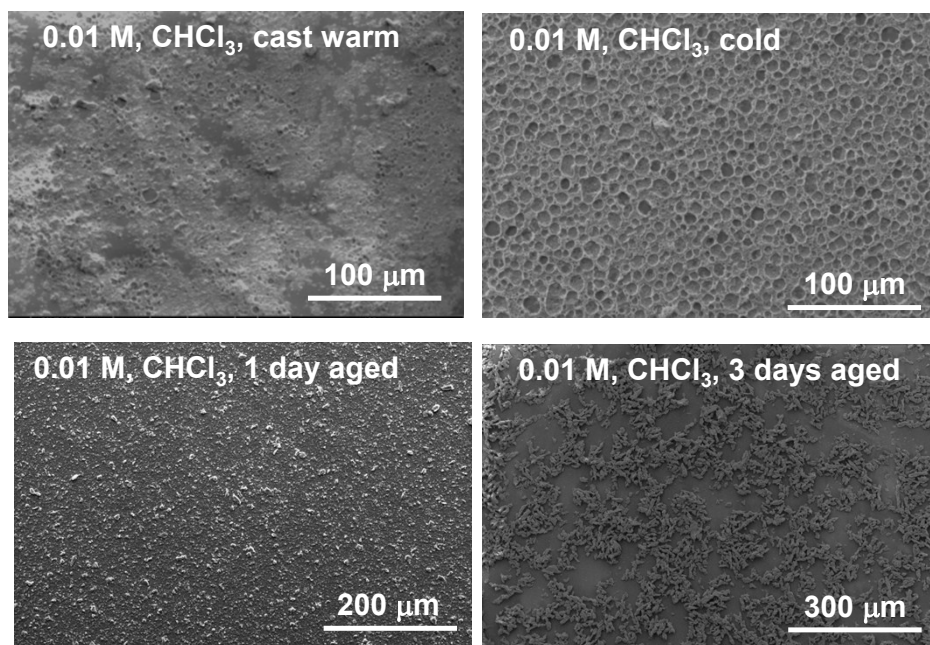
**Figure S7.** Thin films of complex **3b** made by drop casting solutions in ODCB (heat and cool) and  $\text{CHCl}_3$  (72 hours aged). [**3b**] = 0.01 M.



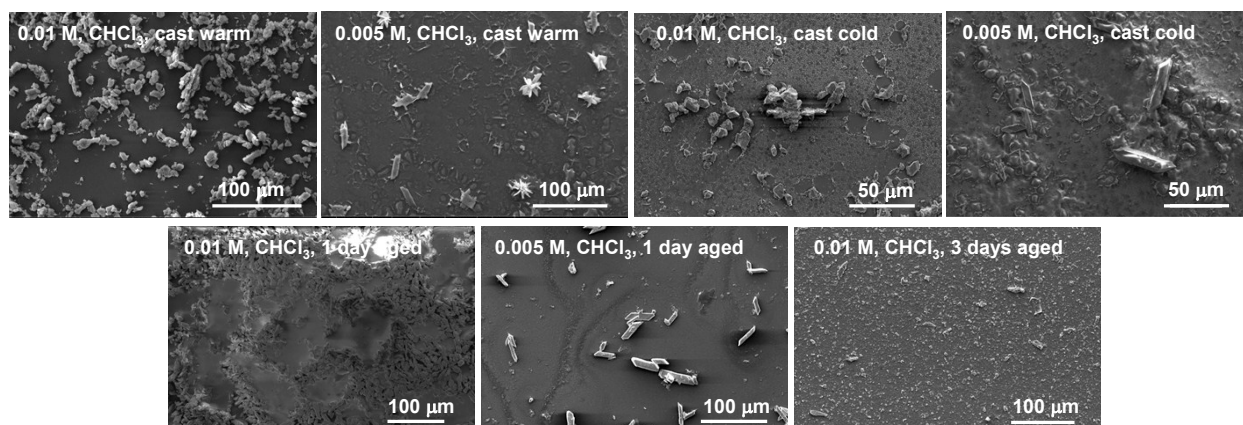
**Figure S8.** Thin films of complex **3b** made by drop casting solutions in  $\text{CHCl}_3$  at different concentrations and aging times.



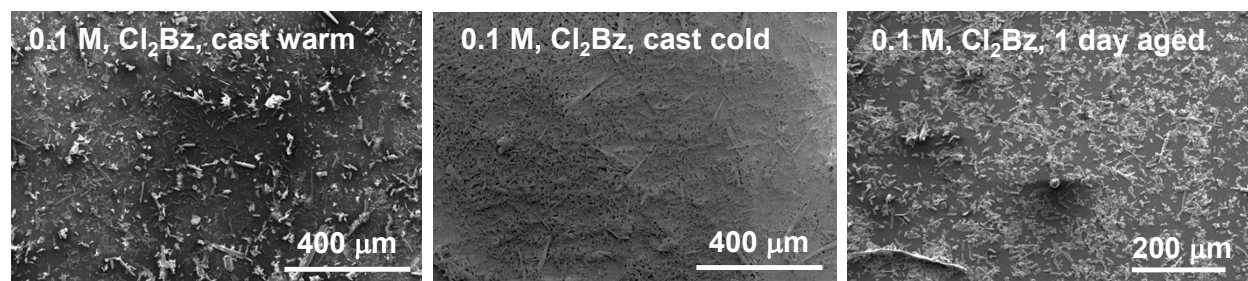
**Figure S9.** SEM images of films made by spin coating solutions of complex **3b** in ODCB at different aging times. [**3b**] = 0.01 M.



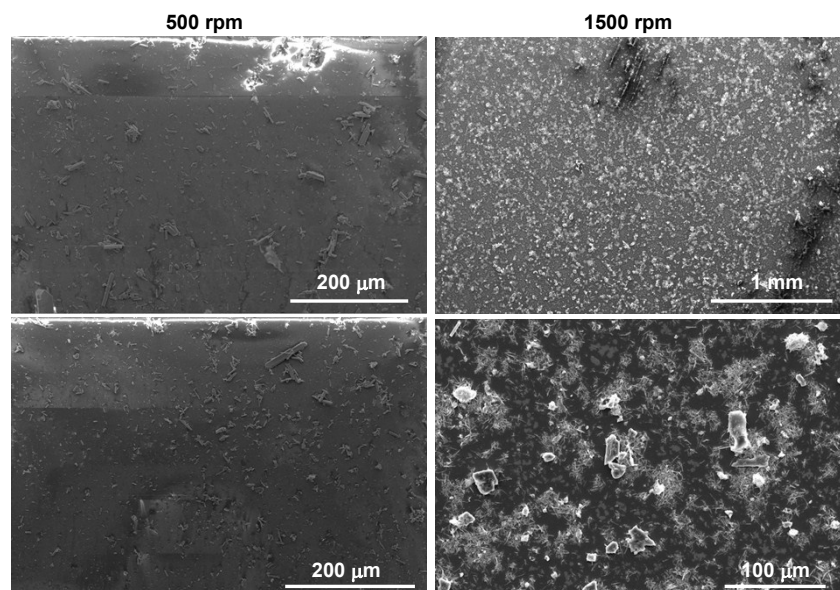
**Figure S10.** SEM images of films made by drop casting solutions of complex **3c** in CHCl<sub>3</sub> at different conditions and aging times.



**Figure S11.** SEM images of films made by drop casting solutions of complex **3d** in CHCl<sub>3</sub> at different concentrations and conditions.



**Figure S12.** SEM images of films made by drop casting solutions of complex **3d** in ODCB. [**3d**] = 0.1M



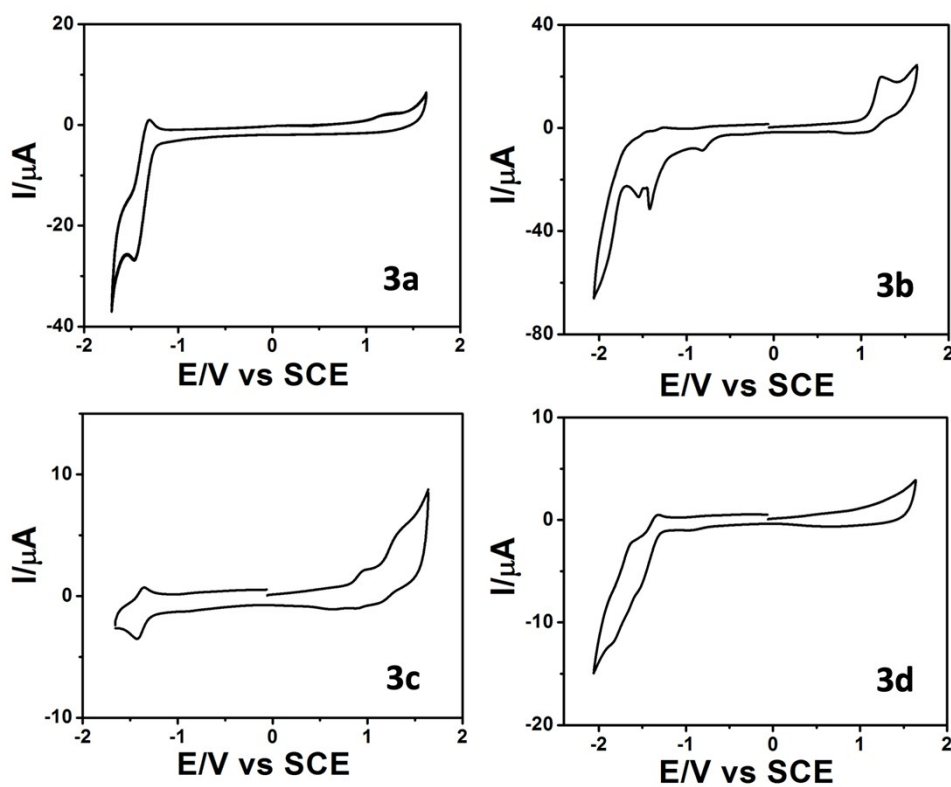
**Figure S13.** SEM images of films made by spin coating solutions of complex **3d** in ODCB at different spin rates. [**3d**] = 0.1M

**Table S14.** PXRD parameters for complexes **3a-3d**.

Complex	Crystal system	Space group	A(Å)	B(Å)	C(Å)	Alpha(°)	Beta(°)	Gamma(°)	Cry (nm)	Rwp
<b>3a</b>	Monoclinic	P21(4)	15.353	3.790	13.567	90	128.770	90	333	18.1
<b>3b</b>	Triclinic	P-1(2)	2.999	24.897	40.0052	89.653	90.129	90.078	366	14.9
<b>3c</b>	Orthorombic	P222(16)	35.4967	12.1729	5.006765	90	90	90	156	10.2
<b>3d</b>	Triclinic	P-1(2)	13.5495	22.4959	27.0455	83.99	87.85	90.7	60	11.5

**Table S.15.** Simulated values of Pt---Pt and  $\pi$ - $\pi$  in the self-assembled structures of **3a**, **3b**, **3c**, **3d**. **py1** represents the pyridine ring in the tridentate ligand, **py2** represents the pyridine ring in the ancillary ligand, **trz** stands for the triazole moiety, **thio1** represents the closest thiophene to the Pt(II) center, and so on.

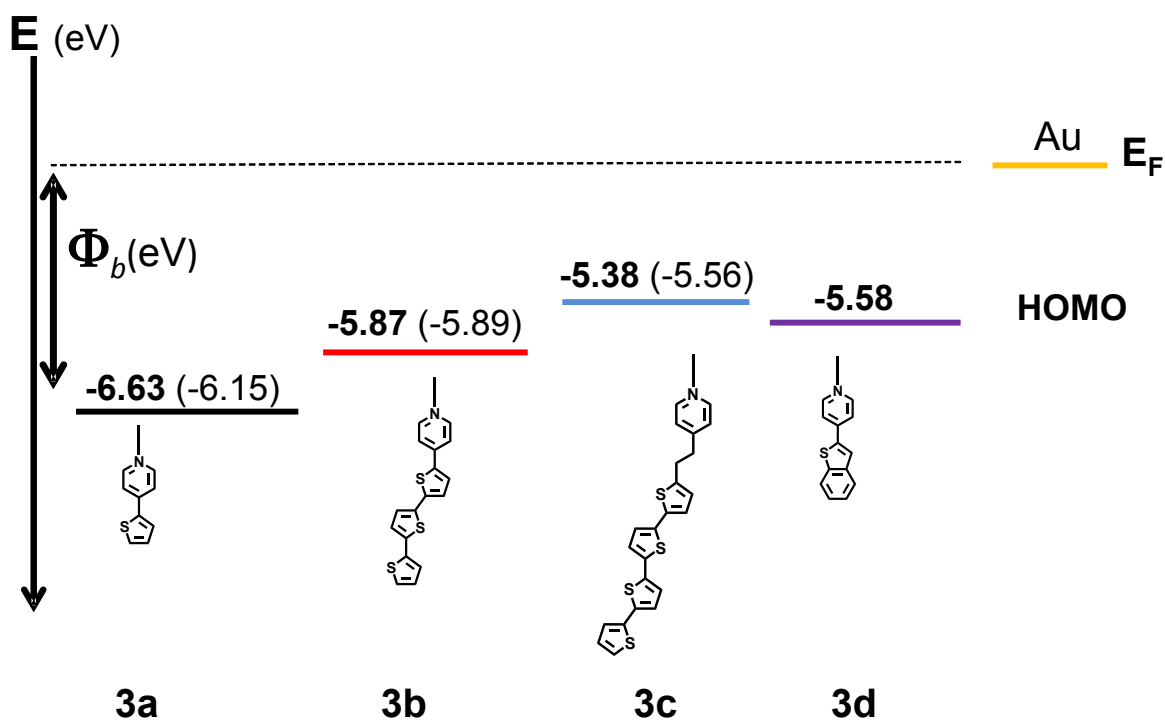
Complex	Pt---Pt(Å)	$\pi$ - $\pi$ (Å)	$\pi$ - $\pi$ (Å)	$\pi$ - $\pi$ (Å)
<b>3a</b>	3.79	3.79 (py1-py1)	3.79 (py2-py2)	3.79-3.79 (thio-thio)
<b>3b</b>	6.71	5.22 (thio1-py2)	5.53 (py1-thio1)	4.90 (py1-trz)
<b>3c</b>	11.44	4.41 (thio2-trz)	5.97 (thio4-thio4)	
<b>3d</b>	3.21	3.12 (py1-py2)	2.96 (trz-trz)	



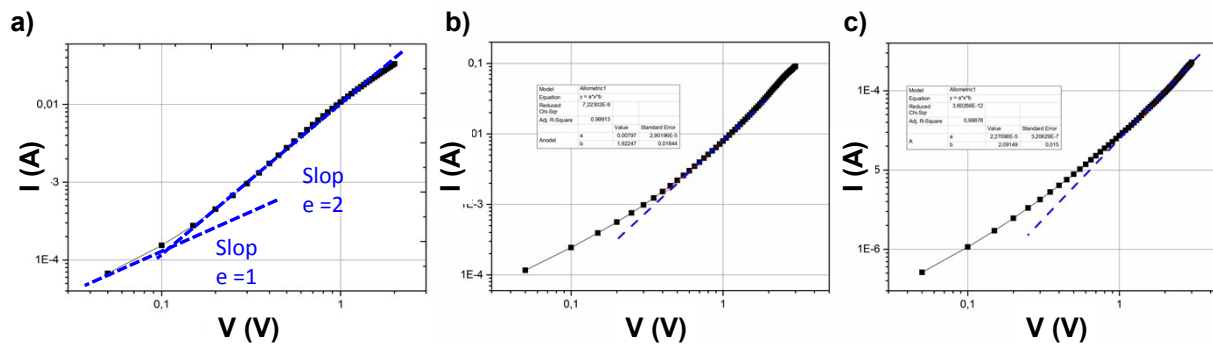
**Figure S14.** Cyclic voltammograms of complexes **3a-d**.

**Table S16.** Electrochemical data, energy levels and optical energy bandgap for complexes **3a-3d**

Complex	$E_{\text{ox}}$ (V)	$E_{\text{red}}$ (V)	HOMO (eV)	LUMO (eV)	$E_{\text{op\_gap}}^{\text{op}}$ (eV)
<b>3a</b>	1.5	-1.304	-6.15	-3.62	2.53
<b>3b</b>	1.364	-1.3, -1.46	-5.89	-3.97	1.92
<b>3c</b>	0.97, 1.32	-1.39	-5.56	-3.81	1.75
<b>3d</b>	No peaks by CV	-1.4, -1.71	-5.58	-3.47	2.11



**Figure S15.** HOMO levels of complexes **3a-3d**.  $\Phi_b$  represents the injection barrier for holes. In brackets are shown the values calculated from the cyclic voltammetry data and in bold, the values calculated from DFT.

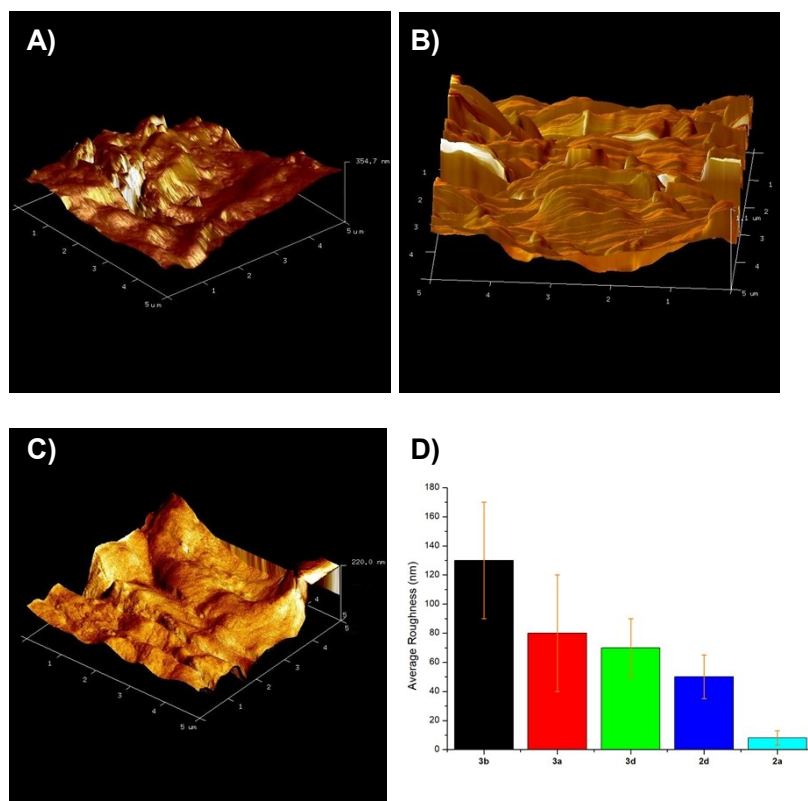


**Figure S16.** Representative IV curves of complexes **3a**, **3b** and **3d**.

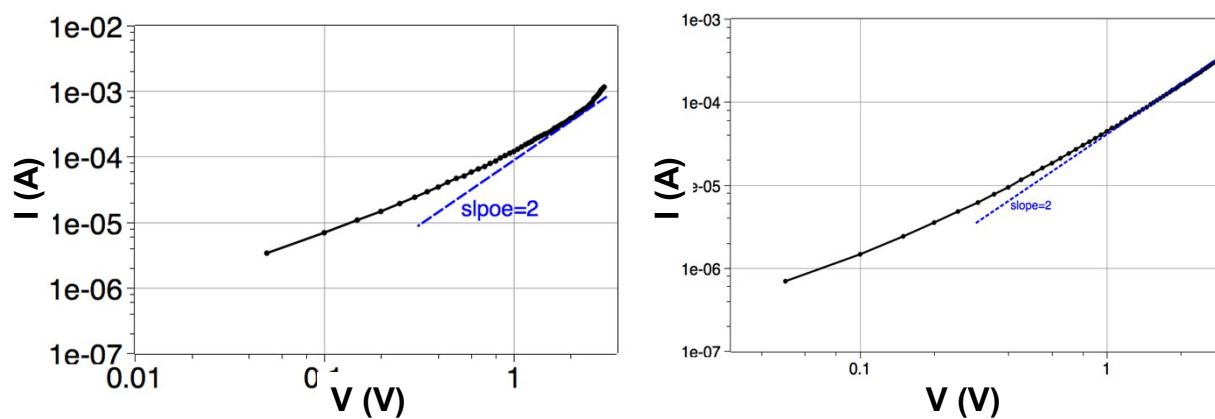
**Table S17.** Device characteristics

Derivative	Roughness (nm)	Mobility ( $\text{cm}^2\text{V}^{-1}\text{s}^{-1}$ )	Number of working diodes
<b>3a</b>	80±44	$(3.5\pm 0.6)\times 10^{-3}$	20
<b>3b</b>	130±43	$(6.0\pm 0.2)\times 10^{-4}$	2
<b>3d</b>	70±20	$(1.1\pm 0.1)\times 10^{-3}$	8
<b>2d</b>	50±12	$(3.4\pm 0.1)\times 10^{-5}$	11
<b>2a</b>	10±5	$(3.3\pm 0.4)\times 10^{-7}$	4

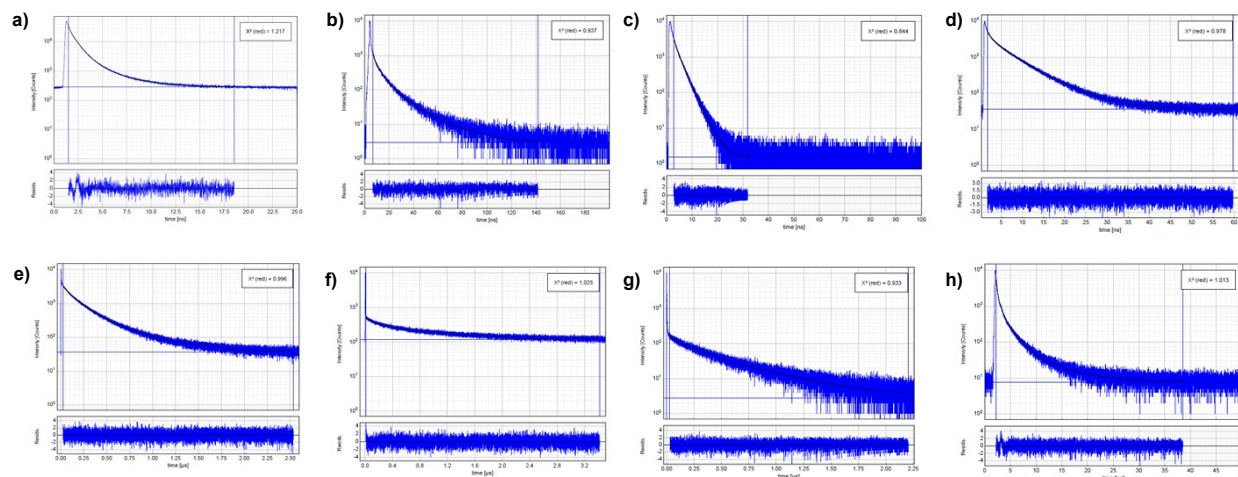




**Figure S17.** 3D AFM images of complexes **3a** (A), **3b** (B) and **3c** (C) and the plot of the average roughness for each complex and ligands.



**Figure S18.** Representative IV curves of the ligands **2a** and **2d**.



**Figure S19.** Excited state life time of complexes 3a (a), 3b (b), 3c (c) and 3d (d) in solution and 3a (e), 3b (f), 3c (g) and 3d (h) in powder.

## References

- <sup>1</sup>C. Adamo and V. Barone, *The Journal of Chemical Physics*, 1999, 110, 6158-6170.
- <sup>2</sup>J. P. Perdew, K. Burke and M. Ernzerhof, *Phys. Rev. Lett.*, 1997, 78, 1396-1396.
- <sup>3</sup>J. P. Perdew, K. Burke and M. Ernzerhof, *Phys. Rev. Lett.*, 1996, 77, 3865-3868.
- <sup>4</sup>M. M. Francl, W. J. Pietro, W. J. Hehre, J. S. Binkley, M. S. Gordon, D. J. DeFrees and J. A. Pople, *The Journal of Chemical Physics*, 1982, 77, 3654-3665.
- <sup>5</sup>M. Dolg, U. Wedig, H. Stoll and H. Preuss, *The Journal of Chemical Physics*, 1987, 86, 866-872.
- <sup>6</sup>D. Andrae, U. Häußermann, M. Dolg, H. Stoll and H. Preuß, *Theoretica chimica acta*, 1990, 77, 123-141.
- <sup>7</sup>M. J. Frisch, G. W. Trucks, H. B. Schlegel, G. E. Scuseria, M. A. Robb, J. R. Cheeseman, G. Scalmani, V. Barone, B. Mennucci, G. A. Petersson, H. Nakatsuji, M. Caricato, X. Li, H. P. Hratchian, A. F. Izmaylov, J. Bloino, G. Zheng, J. L. Sonnenberg, M. Hada, M. Ehara, K. Toyota, R. Fukuda, J. Hasegawa, M. Ishida, T. Nakajima, Y. Honda, O. Kitao, H. Nakai, T. Vreven, J. A. Montgomery Jr., J. E. Peralta, F. Ogliaro, M. J. Bearpark, J. Heyd, E. N. Brothers, K. N. Kudin, V. N. Staroverov, R. Kobayashi, J. Normand, K. Raghavachari, A. P. Rendell, J. C. Burant, S. S. Iyengar, J. Tomasi, M. Cossi, N. Rega, N. J. Millam, M. Klene, J. E. Knox, J. B. Cross, V. Bakken, C. Adamo, J. Jaramillo, R. Gomperts, R. E. Stratmann, O. Yazyev, A. J. Austin, R. Cammi, C. Pomelli, J. W. Ochterski, R. L. Martin, K. Morokuma, V. G. Zakrzewski, G. A. Voth, P. Salvador, J. J. Dannenberg, S. Dapprich, A. D. Daniels, Ö. Farkas, J. B. Foresman, J. V. Ortiz, J. Cioslowski and D. J. Fox, *Journal*, 2009.
- <sup>8</sup>N. M. O'Boyle, A. L. Tenderholt and K. M. Langner, *J. Comput. Chem.*, 2008, 29, 839-845.